ACS APPLIED MATERIALS & INTERFACES

Research Article

www.acsami.org

Gravure-Printed Sol–Gels on Flexible Glass: A Scalable Route to Additively Patterned Transparent Conductors

William J. Scheideler, Jaewon Jang, Muhammed Ahosan Ul Karim, Rungrot Kitsomboonloha, Andre Zeumault, and Vivek Subramanian*

Department of Electrical Engineering and Computer Sciences University of California, Berkeley Berkeley, California 94720-1764, United States

Supporting Information

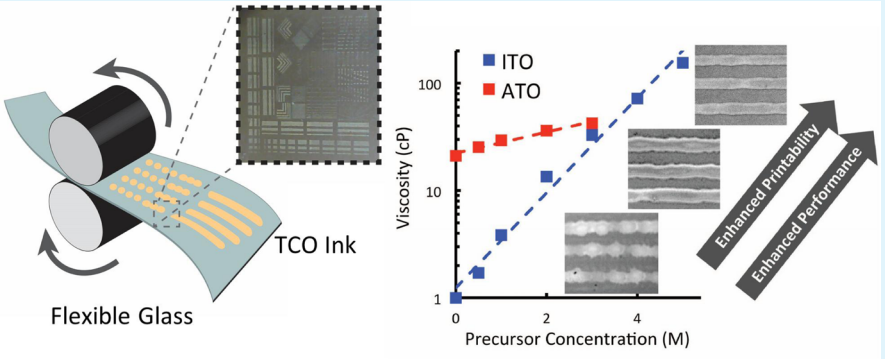

ABSTRACT: Gravure printing is an attractive technique for patterning high-resolution features (<5 μm) at high speeds (>1 m/s), but its electronic applications have largely been limited to depositing nanoparticle inks and polymer solutions on plastic. Here, we extend the scope of gravure to a new class of materials and on to new substrates by developing viscous sol–gel precursors for printing fine lines and films of leading transparent conducting oxides (TCOs) on flexible glass. We explore two strategies for controlling sol–gel rheology: tuning the precursor concentration and tuning the content of viscous stabilizing agents. The sol–gel chemistries studied yield printable inks with viscosities of 20–160 cP. The morphology of printed lines of antimony-doped tin oxide (ATO) and tin-doped indium oxide (ITO) is studied as a function of ink formulation for lines as narrow as 35 μm, showing that concentrated inks form thicker lines with smoother edge morphologies. The electrical and optical properties of printed TCOs are characterized as a function of ink formulation and printed film thickness. XRD studies were also performed to understand the dependence of electrical performance on ink composition. Printed ITO lines and films achieve sheet resistance (R_s) as low as 200 and 100 Ω/□, respectively ($\rho \approx 2 \times 10^{-3}$ Ω-cm) for single layers. Similarly, ATO lines and films have R_s as low as 700 and 400 Ω/□ with $\rho \approx 7 \times 10^{-3}$ Ω-cm. High visible range transparency is observed for ITO (86–88%) and ATO (86–89%). Finally, the influence of moderate bending stress on ATO films is investigated, showing the potential for this work to scale to roll-to-roll (R2R) systems.

KEYWORDS: *Gravure printing, sol–gel conductor, transparent conductor, solution-processed, additive patterning*

INTRODUCTION

Transparent conducting oxide (TCO) electrodes are essential components in ubiquitous thin film devices, including solar cells,[1,2] LEDs,[3] touch screens,[4] displays,[5−7] and transparent thin film transistors (TTFTs).[8] Conventional fabrication approaches for patterning TCOs typically require vacuum technologies and subtractive processing, which result in low material utilization and limit the viable material set to TCOs with suitable etch selectivity. Solution-processed TCO electrodes can potentially leverage the advantages of additive processing techniques, such as printing technologies, to greatly improve material utilization and enhance throughput for patterned TCO films at a reduced cost.[9] These benefits are particularly relevant to leading transparent conductors based on indium and silver which exist in limited earth abundance,[10] but have rapidly growing applications in photovoltaics and display technology.

Various printing-based patterning techniques have been considered for printed electronics, ranging from digital printing techniques such as inkjet printing to high-speed contacting printing techniques such as gravure printing.[11] Serial patterning methods, such as inkjet printing, utilize direct digitally driven writing of a pattern, which allows easy design modifications but limits throughput compared to roll-to-roll (R2R) parallel patterning techniques such as screen, flexographic, and gravure printing. There have been significant works and well-established

Received: January 7, 2015
Accepted: May 27, 2015
Published: May 27, 2015

DOI: 10.1021/acsami.5b00183
ACS Appl. Mater. Interfaces 2015, 7, 12679–12687

theories for inkjet printing of metal oxide sol–gels.[12] In contrast, there has been limited research on direct patterning of metal oxide materials using scalable parallel patterning such as gravure. Puetz et al. demonstrated gravure-patterned ITO using nanoparticle inks on plastic foils with feature size of approximately 100 μm, but performance was limited by low process temperatures (<180 °C) and high porosity of the nanoparticle films.[13,14] To our knowledge, these are the only patterned solution-processed TCOs demonstrated by a highly scalable roll-based method. Alternative transparent conductors such as metal nanowire networks and conductive polymer materials (PEDOT:PSS) exist, but these systems are less chemically and mechanically stable[15] and lack suitable work functions for efficient electron injection.[16] In this work, we address the technological need for high-resolution additively patterned TCOs by developing gravure-printed sol–gel transparent conductors.

Gravure printing is a competitive technique for patterning high-resolution (<5 μm) features at high speeds ($\geq$ 1m/s).[17] However, the scope of gravure printed electronic materials has previously been limited to polymeric organic inks and nanoparticle inks. A principal reason for this has been the limited thermal capability of transparent plastic substrates, which have poor dimensional stability above 200 °C. However, thin glass substrates offer a favorable combination of excellent thermal stability ($T_g \approx 600$ °C), ultrasmooth surface quality (R_a < 0.5 nm) for device fabrication, and reasonable flexibility,[18] enabling many new applications and scalable R2R manufacturing methods for high performance materials requiring processing temperatures in the range of 400–600 °C. In addition to thermal stability, thin glass substrates provide mechanical flexibility, which is essential for facilitating R2R contact printing such as gravure.[19] This flexibility allows substrates to conform to roll runout, forming an intimate contact for printing high-resolution lines and films at a high speed, as illustrated in Figure 1. Because of its higher Young's modulus (E = 70 GPa[19]), glass also limits substrate deformation during printing and thermal processing to enhance registration. Therefore, thin glass substrates are promising candidates for flexible, printed electronics technologies that need high process temperatures.

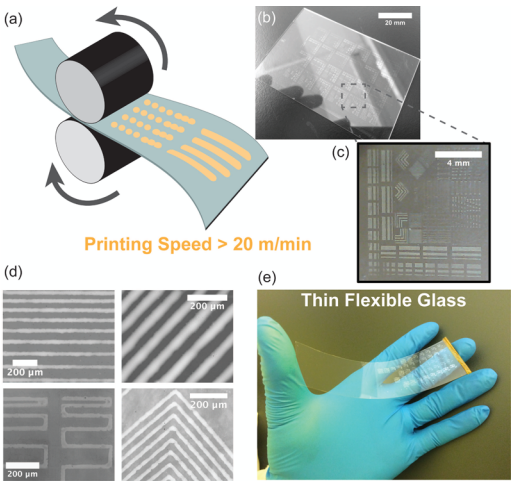

Figure 1. Schematic of gravure printing process on thin flexible glass with metal gravure cylinders (a). Glass substrate with patterned ATO (2M) printed at 0.4 m/s (24 m/min). Printed ATO features on glass (c). Fine lines (35um) printed with ITO (top-left, bottom-left) and ATO (top-right, bottom-right) on flexible glass substrates (e).

Here, we utilize flexible glass substrates to realize high-resolution conductive (500 S/cm) printed TCO electrodes with line widths as small as 35 μm via highly concentrated sol–gel precursor inks. The rheology of sol–gel precursors is studied and controlled via precursor concentration and cosolvent addition to guide the development of printable gravure inks and fabricate uniform, smooth electrodes. The line morphology, optical transparency, crystallinity, and electrical performance of tin-doped indium oxide (ITO) electrodes and antimony-doped tin oxide (ATO) electrodes are studied as a function of the ink formulation. Finally, the electrical performance under flexion fatigue is examined to understand the mechanical reliability of printed sol–gel conductors.

RESULTS AND DISCUSSION

Gravure Ink Design. The sol–gel process is a well-known strategy for forming TCO films directly from liquid phase precursors. However, formulating sol–gel inks that exhibit both optimal material properties and suitable rheology for roll-based printing is a challenge. Solution-processed TCOs formed by spin-coating have recently reached record conductivities[20] that approach the performance of sputtered ITO while utilizing metal salts.[21] While these sol–gel chemistries yield high performance TCOs, the sol–gel precursors' rheology is currently unsuitable for gravure printing. Common metal salt sol–gel schemes using aging[22] or stabilizer addition[23] have also been used to increase viscosity slightly from 1 cP to about 10 cP,[24] but these viscosities remain too low for the gravure printing herein. Formulating an ink for high-resolution gravure printing requires viscosities near 100 cP to produce fine lines with smooth edges, few pinholes, and controllable width.[25] Furthermore, in addition to viscosity (η), the surface tension (γ) of an ink plays an important role in high-resolution patterning, as it balances viscous forces during ink transfer and pattern formation. This balance of viscous forces and surface tension forces can be represented at a particular printing speed (U) as the nondimensional capillary number ($Ca = \eta U/\gamma$), offering a useful metric for predicting printability of an ink, as detailed in ref 17. At very low capillary number, ($Ca \ll 1$) pattern fidelity is deteriorated by ink drag-out from the cells and at very high capillary number ($Ca \gg 1$) inefficient doctoring leaves ink in nonpatterned areas. Optimal printing can be achieved by adjusting printing speed and ink parameters to make $Ca \approx 1$.[17] Therefore, to achieve optimal pattern formation at a particulary printing speed (often limited by printing machine capabilities) requires appropriate tuning of the fluid viscosity and surface tension of an ink.

Sol–Gel Ink Formulation. In this work, we explore methods for controlling viscosity and surface tension of metal salt-based sol–gel inks to effectively access optimal printing conditions. In the first method, varying the concentration of the precursor tunes the sol–gel ink viscosity, similar to methods used for nanoparticle dispersions and polymer solutions. This principle is illustrated in Figure 2a for two electronically functional sol–gel inks, including indium tin oxide (ITO) and antimony-doped tin oxide (ATO), each of which is enhanced to gravure-printable viscosities (20–100 cP). Viscosity depends exponentially on precursor concentration in the case of the ITO and ATO dissolved in a strongly complexing solvent such as pure acetylacetone (AcAc) or pure ethylene glycol (EG). In contrast, sols dissolved in a mixture of EG and ethanol

DOI: 10.1021/acsami.5b00183
ACS Appl. Mater. Interfaces 2015, 7, 12679–12687

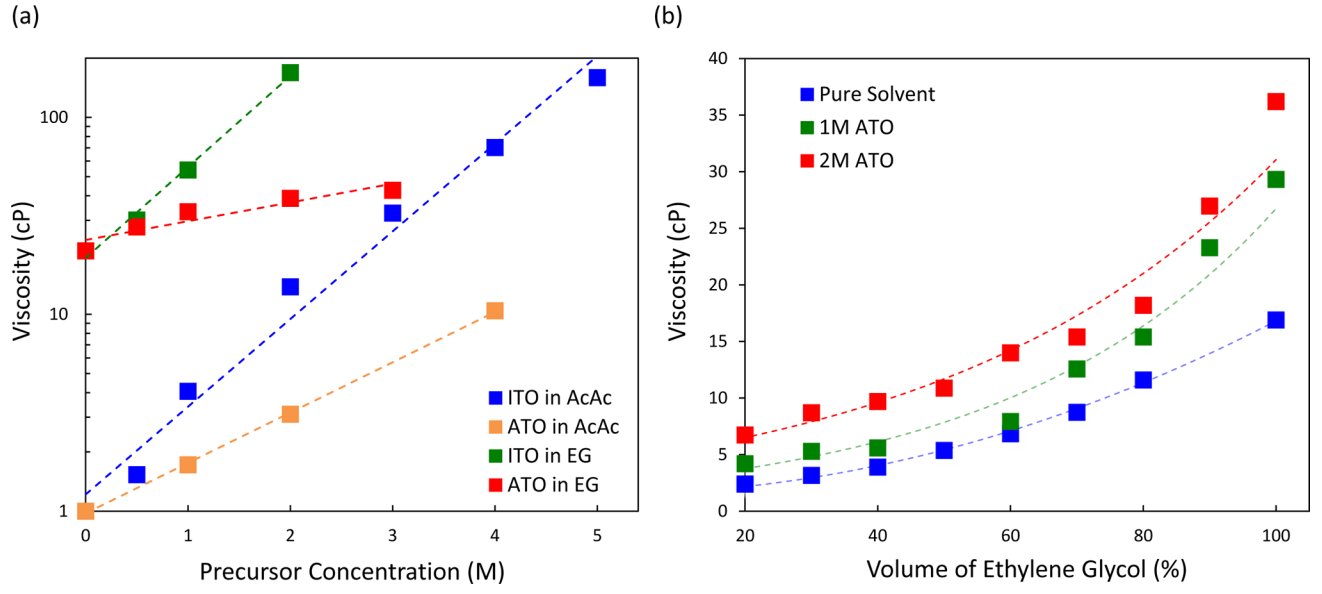

Figure 2. (a) Measured viscosity (shear rate = 15 s^{-1}) vs precursor concentration of ITO and ATO inks dissolved in the indicated solvents. (b) Viscosity (shear rate = 15 s^{-1}) of ATO inks vs solvent composition, plotted as a function of the volumetric fraction of EG in an ethanol/EG mixture.

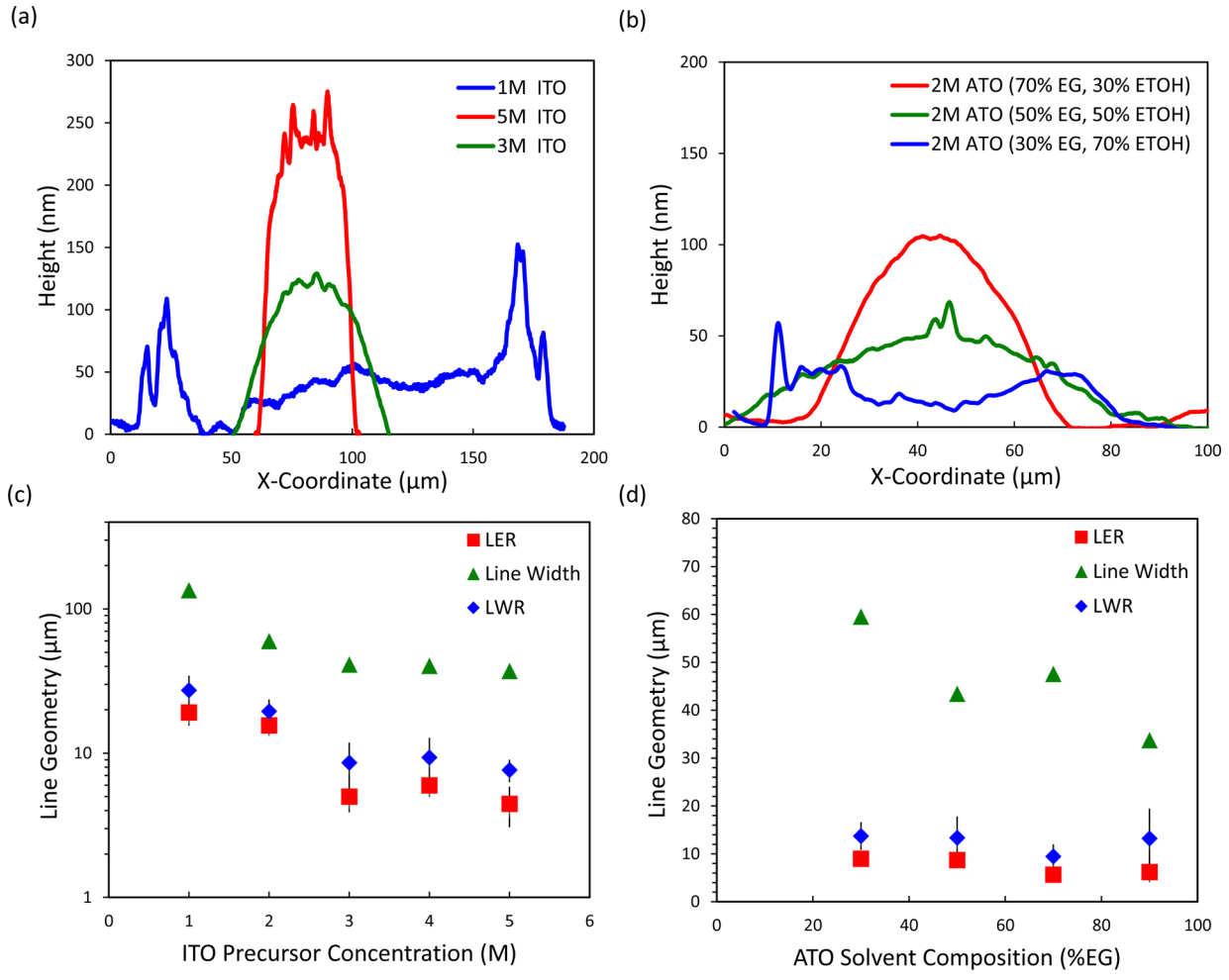

Figure 3. (a) Line-profiles measured for 1, 3, and 5 M ITO inks in AcAc printed with 20 μm cells at 0.4 m/s and 100 N printing force. (b) Line profiles for 2 M ATO inks with various solvent compositions. (c) Line width, line-edge-roughness (LER), and line-width-roughness (LWR) for ITO inks of varying concentration in AcAc. (d) Line width, line-edge-roughness (LER), and line-width-roughness (LWR) for 2 M ATO inks of varying solvent composition (EG %).

DOI: 10.1021/acsami.5b00183
ACS Appl. Mater. Interfaces 2015, 7, 12679−12687

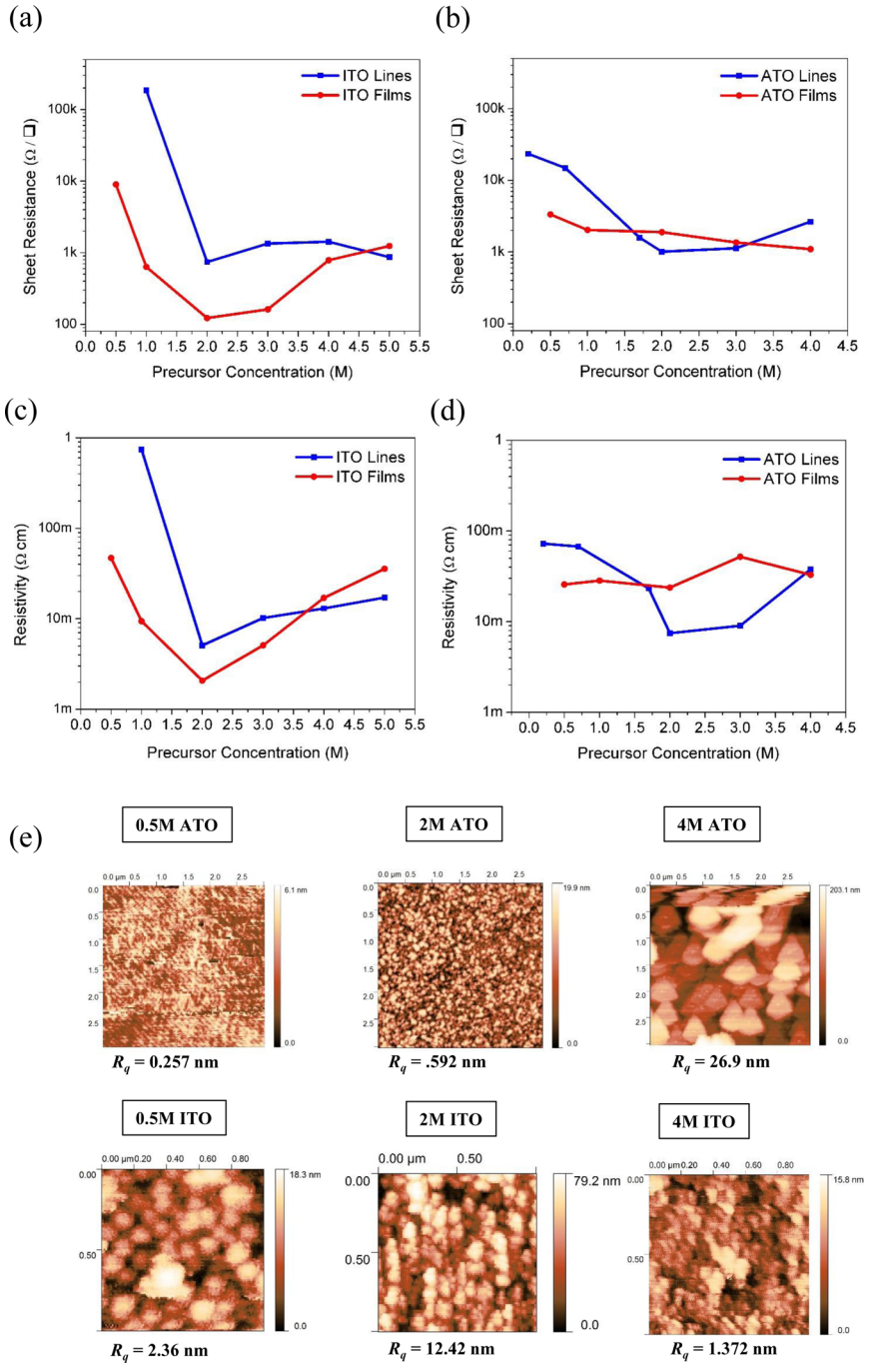

Figure 4. Measured sheet resistance of ITO (a) and ATO (b) as a function of precursor concentration for lines (black) and blanket films (red). (c,d) Resistivity vs precursor concentration of ITO and ATO. (e) Surface morphology of printed films from 0.5, 2, and 4 M ATO and ITO precursors measured by AFM.

(ETOH) show a weaker dependence of viscosity on concentration, increasing less relative to the neat viscosity. Observations of thixotropic behavior, such as counterclockwise hysteresis loops, in measurements of shear stress (Supporting Information Figure S1) may also reflect the formation of a solvated network in concentrated inks.[26] The range of viscosities accessed by this method is highlighted in Figure 2a, showing how concentrated metal salt sol–gels can reach viscosities near 100 cP to allow high resolution printing. While it is true that alkoxide chemistries can give similar tunability in fluid properties, their high cost relative to metal salts could inhibit large scale printed electronics applications. Although this method effectively tuned the viscosity over 2 orders of magnitude, the surface tension of inks remained nearly constant over a wide range of metal concentrations (Supporting Information Figure S2). This property is attractive for facilitating the use of similar surface treatments for different ink concentrations.

Sol–gel inks formulated by this method were gravure printed at similar speeds and contact pressure, with equivalent surface treatments and drying conditions. The three-dimensional line morphology of these prints was studied to understand the effect of increasing *Ca* through viscosity tuning. Figure 3a illustrates the profiles of gravure-printed lines as a function of the metal

DOI: 10.1021/acsami.5b00183
ACS Appl. Mater. Interfaces 2015, 7, 12679–12687

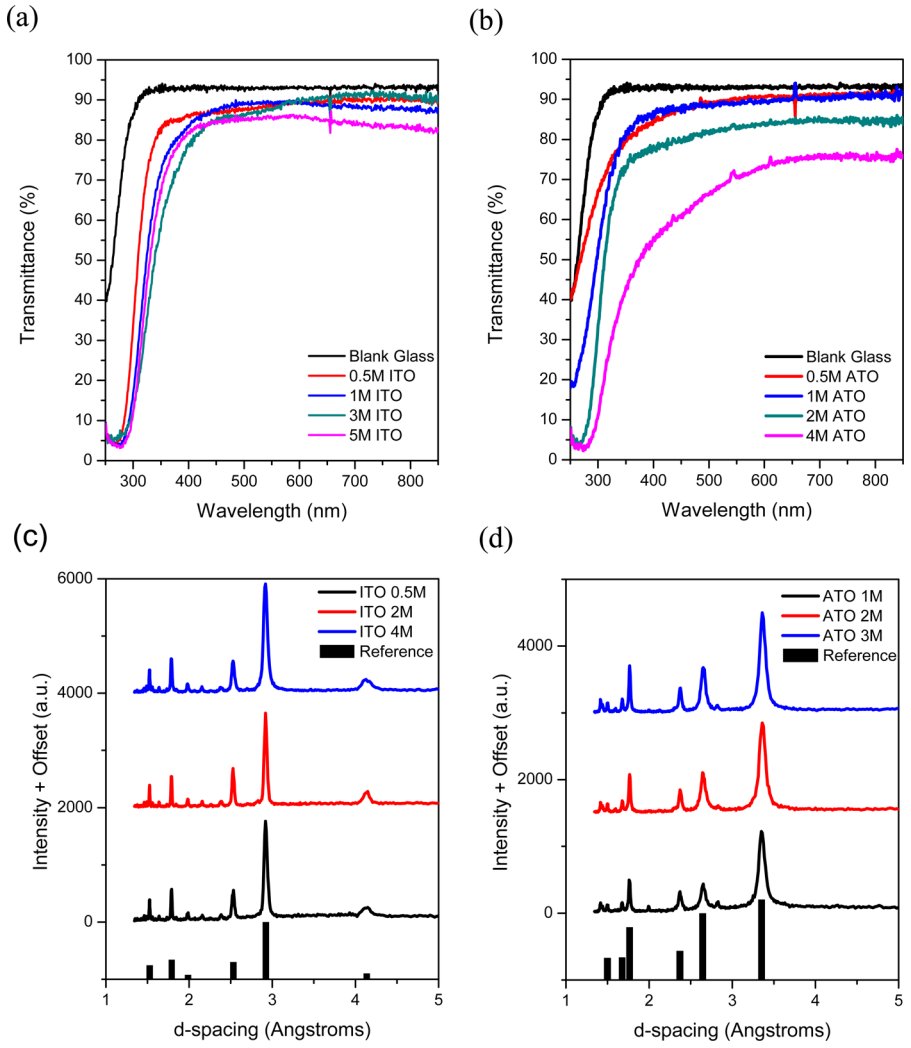

Figure 5. (a) Transmittance spectra of ITO printed films as a function of concentration of ITO precursor ($In(NO_3)_3$ and $SnCl_4$ in AcAc). (b) Transmittance spectra of ATO printed films as a function of concentration of ATO precursor. Transmittance of the bare glass substrate is shown for reference. GIXD spectra of ITO films (c) and ATO films (d) plotted with reference signals indicated below (LPF no. 1216580, ICSD no.154961).[33,34]

concentration of ITO sol–gels in pure AcAc. The observed line profiles (Figure 3a) suggest that more viscous, high concentration inks lead to a reduction in the spreading rate and a suppression of the coffee ring effect, forming thicker dome-shaped or parabolic lines. Another appropriate explanation is that higher concentration inks have a smaller volumetric percentage of solvents, which evaporate during drying, elevating the viscosity so that the 2D pattern is frozen into its final geometry by a sol–gel transition.[26,27] The line widths (Figure 3b) of gravure-printed ITO sol–gels shows that significant spreading occurs after ink is transferred to the substrate for low precursor concentrations (<3M). In comparison, concentrated inks give better control over the line width and show significantly lower line-edge-roughness/line-width-roughness (Figure 3c), a reflection of stable line formation. These trends reflect the enhanced printability of concentrated inks, as predicted by the longer relaxation times following application of shear stress as shown in creep-recovery tests (Supporting Information Figure S1).

Controlling the solvent composition of sol–gel precursors is a complementary method to enhance the *Ca* and span the ink design space for optimizing printability. This second method is demonstrated here for ATO sol–gel inks with a binary solvent of EG and ethanol. Figure 2b illustrates the increase in viscosity obtained by adding EG to ATO sol–gels in ethanol. Sol–gel inks with different precursor concentrations show similar enhancements in viscosity, reaching a suitable range for gravure printing at concentrations between 1 and 2 M. Although the viscosity of the binary solvent ATO inks does not increase exponentially with this mechanism, this cosolvent system has the added benefit of reducing coffee-ring effects, which typically result in sharply peaked line edges and nonuniform deposition.

Cosolvent-based systems are a well-known method for managing the coffee-ring effect in printed inks. Cosolvents can induce recirculating flows, which homogenize particle concentrations to yield uniform films and smooth line profiles.[28] In the case of the ATO inks utilized in this study, ink wetting on the substrate significantly changes with respect to the EG content, as expected from the higher surface tension of EG (48.6 mN/m) vs ethanol (21.8 mN/m).[29] The increased contact angle, originating from the higher surface tension of EG, may slow preferential evaporation at the edges due to the increased volume of ink per unit area. The reduced evaporation rate at the edges also decreases potential spreading originating

DOI: 10.1021/acsami.5b00183
ACS Appl. Mater. Interfaces 2015, 7, 12679–12687

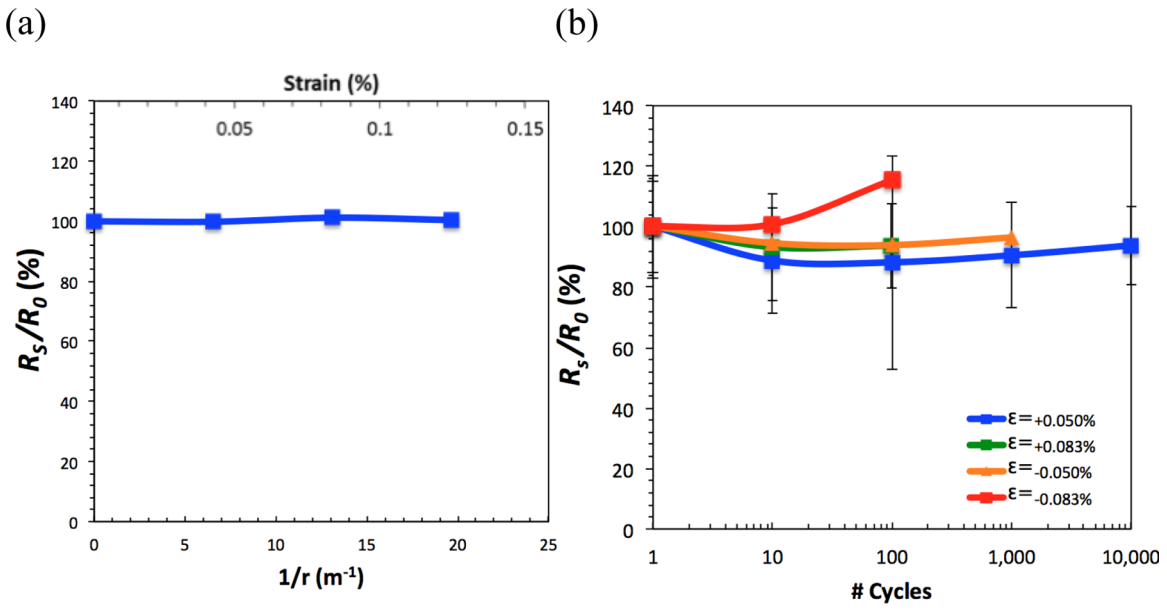

Figure 6. (a) Normalized sheet resistance of ATO lines (40 μm width) as a function of inverse bending radius and strain for uniaxial bending stress applied along the axis of the printed lines. (b) Normalized sheet resistance vs number of cycles of uniaxial bending stress for compressive (+) and tensile (−) strain.

from the outward liquid flow to replace evaporated solvent. As a result, coffee-ring-less uniform ATO electrodes were successfully printed with inks of 50−70% EG in ethanol (Figure 3b) by using this method to access the optimal range of *Ca* shown in Figure 2. These results indicate that this second method of ink formulation consisting of a cosolvent system is a viable technique to obtain favorable line morphologies at lower precursor concentrations (1−2 M) than are required for single solvent concentrated inks (3−5M). Collectively these two methods offer useful tools to span the parametric space of fluid parameters that guide gravure ink design. This capability allows one to optimize printable sol−gel inks for arbitrary printing speeds and surfaces. However, for these functional inks it is also important to consider the impact of ink design on material performance.

Electrical Performance of Sol−Gel Inks. The electrical performance of the printed sol−gels was characterized as a function of ink formulation to understand the impact of rheological ink optimization on the functional material properties. The sheet resistance and thickness were directly measured for printed inks formulated from concentrated precursor method and cosolvent method. Figure 4 illustrates the sheet resistance and resistivity of ITO and ATO sol−gels as a function of the sol−gel precursor concentration for different gravure cell sizes. In both cases, sheet resistance is improved at higher precursor concentrations as thicker solid films are deposited. ITO features with optimized annealing conditions are highly conductive, with sheet resistance (R_S) as low as 100 Ω/□ for single-layer blanket films and 200 Ω/□ for lines. ATO sol−gels formed from Sn(II) and Sb(III) salts have slightly lower performance, but allow printing of conductive lines with R_S as low as 700 Ω/□. The resistivity of these single layer gravure-printed features compares favorably to sol−gel-derived films formed by other coating method such as dip-coating and spin-coating despite the fact that these methods use multilayer films of 5−10 layers that effectively fill cracks and pinholes to ensure film continuity. Resistivity as low as 2×10^{-3} Ω-cm ($\sigma \approx 500$ S/cm) is achieved for single-layer printed ITO. To our knowledge, this is the best conductivity achieved for additively patterned solution-processed TCO features (Supporting Information Table S2). The gravure printed ATO lines have a resistivity of 7×10^{-3} Ω-cm (143 S/cm), which is comparable to other reports of solution-processed ATO.[22]

The measured resistivity is observed to be a function of the ink concentration, which may related to the variation in film thickness. Film thickness should affect the morphology of the sol−gel-derived film in multiple ways. In the case of polycrystalline TCO films such as ITO and ATO, it has been reported that crystallite size increases with film thickness for a given composition and annealing process, leading to improved conductivity.[31,32] In the case of gravure-printed ITO, the conductivity of the films improves with precursor concentration and is optimized at approximately 2M. An analysis of the primary (222) peak fwhm in the XRD spectra (Figure 5c) of the ITO films indicates that crystallinity is optimized at 2 M and decreases with increasing precursor concentration. AFM imaging (Figure 4e) also shows larger crystallites in 2 M ITO films than in thicker 4 M films. ATO resistivity does not show a strong optimum at intermediate concentrations, but does demonstrate slight degradation at very high concentrations. In the XRD spectra (Figure 5d) of ATO films, no significant variation is observed in the primary (110) peaks. However, by AFM it is possible to observed that the aggregates in ATO printed films grow larger for higher concentration precursors, leading to an increase in surface roughness and the development of microcracks or voids which could give rise to the increased resistivity.[30]

Transparency of Sol−Gel Inks. The effects of the sol−gel ink formulation on the quality of deposited films can similarly be observed by studying the transparency of the printed features. The sol−gel ink concentration strongly determines the transparency of the gravure-printed sol−gel films. The measured transmittance in the visible range for ATO and ITO films follows similar trends to the conductivity of the material, degrading slightly as the film thickness increases. As illustrated in Figure 5a, the average optical transmittance over

DOI: 10.1021/acsami.5b00183
ACS Appl. Mater. Interfaces 2015, 7, 12679−12687

the visible spectrum (400−800 nm) decreases with increasing concentration of the ITO precursor. For films of optimal conductivity ($t \approx 100-150$ nm), the average transmittance is above 88% for both ITO and ATO. In the case of the highest concentration ink, the films ($t > 300$ nm) have transmittance above 84%. ATO films formed by printing are also highly transparent, with transmittance above 88% for dilute precursors (0.5 M − 1.0M). Concentrated ATO films are less transparent in the visible range and demonstrate a broader UV absorption edge. The printed films microstructure, as shown in Figure 4e, suggests that in high concentration films, large aggregates and microcracks may scatter incident light, reducing transmittance. The mesoscale uniformity is another important parameter for transparent electrode applications. Uniformity was examined by optical microscopy (Supporting Information Figure S4) and SEM (Supporting Information Figure S5), showing that low viscosity inks (1M-2M) give visually uniform films with high uniformity and fewer defects. High viscosity inks (4−5 M) yield films with nonuniformities consisting of spinodal variations in thickness on the scale of 1−5 mm, and, in the thickest films, cracking. While these results do show a limitation to printing thicker TCO layers, they may suggest that alternative annealing strategies (i.e., UV photoannealing) could be employed to improve film quality and manage film stress.

Mechanical Flexibility of Sol−Gel Inks. To understand the mechanical properties of TCO lines printed with the chosen ink formulations, bending tests were performed using TCO patterns and films on flexible willow glass substrates. Figure 6 shows the variation of the sheet resistance of gravure-printed ATO with the bending radius. There is no detectable change in the electrical performance of the film during flexion. As plotted in Figure 6a, the film strain is lower than 0.1% in all cases, since the flexible glass substrate consistently failed at a strain of approximately 0.12−0.15%. The sheet resistance was also measured as a function of the number of bending cycles (Figure 6b) for compressive and tensile strain to study the fatigue properties of the ATO blanket film under flexion. There is negligible change in the sheet resistance of the ATO film under low strains (0.050−0.083%) for up to 10^4 cycles. Compared to the spatial variation in the sheet resistance, the small changes observed in resistance are not considered significant evidence for material degradation. Similar results have been reported for sputtered ITO on 50 μm thick glass substrates for tensile and compressive strain up to 0.21%.[36] Indeed, it is unsurprising that the ATO film is not degraded by moderate bending, considering that the onset of cracking and film degradation is often above 1% strain in sputtered films on plastic foils.[35]

There are two important implications of the mechanical reliability of the ATO films. The first is the viability of R2R processing of flexible glass substrates. The finding that film stress in the ATO layer is low enough to avoid cracking or degradation in sheet resistance is important for allowing extensive web-based processing during which the film and substrate would sustain many cycles of moderate tensile and compressive stress. Indeed, the flexibility characteristics are vital for taking full advantage of the scalability of gravure printing for forming high quality TCO electrodes and films in a high-throughput roll-to-roll process. Second, we expect that these materials and methods provide an effective route to enabling large area applications that require the flexibility, transparency, and lightweight substrates

CONCLUSION

TCO sol−gel inks for gravure printing have been developed for patterning fine features (line widths ∼35−50 μm) and the properties of printed conductors have been investigated as a function of the ink formulation. Ink formulation methodologies based on concentrated sol−gel precursors and cosolvent systems are demonstrated as methods for designing gravure inks with the proper fluid properties to achieve optimal patterning. Sol−gel inks including ITO and ATO prepared with high precursor concentration show improved printing performance due to their increased viscosity (over 100 cP). Patterning metrics such as line-edge roughness and line-width roughness are improved and the 3D morphology is enhanced, producing lines free of coffee-ring features. The electrical performance of printed lines and films also improves with increasing precursor concentration, resulting in single layers with R_S as low as 100 $\Omega/\square$ with average ($400\ \text{nm} \le \lambda \le 800\ \text{nm}$) visible transmittance of 85−88%. Finally, the flexibility of printed ATO electrodes on Corning Willow glass (100 μm thick) was investigated, showing negligible variation in R_s with bending stress and bending fatigue up to 10^4 cycles. Collectively, the results suggest that highly concentrated sol−gel inks offer a promising general route to gravure-printable high-performance metal oxides.

EXPERIMENTAL SECTION

Ink Preparation and Characterization. Sol−Gel inks were mixed at room temperature in air using hydrated metal salts obtained from *Strem Chemicals* ($Sn(IV)Cl_4{\cdot}H_2O$ 98%, $In(NO_3)_3{\cdot}xH_2O$ 99.99%), or Sigma-Aldrich ($Sn(II)Cl_2{\cdot}x(H_2O)$ 99.995%, $SbCl_3{\cdot}x(H_2O)$ 99.99%). Precursors were dissolved in EG (99.8%, *Fisher Scientific*), ethanol (anhydrous, 99.5%, *Sigma-Aldrich*), or AcAc (99.5%, *Sigma-Aldrich*) and sonicated for 1 h until complete dissolution occurred, leaving a clear sol. ITO inks were dissolved in pure AcAc or pure EG and were doped with 10% at. Sn(IV). ATO inks were dissolved in a binary solvent of EG and ETOH and were doped with 8% at. EG content above 20% by volume was required to keep ATO inks stable over long periods of time (more than two months). Ink viscosities were extracted from shear stress during an ascending sweep of shear rates obtained at 30s intervals measured using a Brookfield Cone/Plate Viscometer (DV-III +) for freshly mixed solutions. Pendant drops of various inks were captured at room temperature and surface tension was calculated using the measured inks density and drop geometry extracted in ImageJ.

Printing Process and Annealing. All printing studies were conducted on a sheet fed commercial IGT G1−5 gravure printer. Custom gravure cylinders from Rotadyne Corp were used to pattern arrays of fine lines with 20 μm square shaped wet etched gravure cells (400 l/cm, depth 8 μm, theoretical transfer volume 4.0 mL/m^2). An IGT gravure roller (402.150.433) with 150 μm cells (70 lines/cm, depth 50 μm, theoretical transfer volume 13.5 mL/m^2, screen 53°, stylus 120°) was used to deposit blanket films. A printing speed of 0.4 m/s and a printing force of 100N were used unless otherwise indicated. Glass substrates (100 μm thick Corning Willow glass or 0.5 mm thick Eagle XG glass) were sonicated in acetone, IPA, and DI water before spin-coating a thin layer of PMMA (0.6% in anisole) to adjust the wetting properties; this layer burns off during subsequent thermal processing, and has not been found to impact TCO performance.[37] The PMMA layer (∼10−15 nm thick) was cured at 200°C for 10 min on a hot plate and treated with a UV-Ozone cleaner (Jelight Model 42) for 10 min prior to printing to improve ink transfer from the roller to the substrate. Printed films were dried immediately following printing at 125 (ITO) or 225 °C (ATO) for 10 min, then transferred to a tube furnace for annealing at 400 (ITO) or 500 °C (ATO) for 15 min in air; this high temperature anneal also functions to burn off the PMMA layer. ITO films were postannealed at 300°C in

DOI: 10.1021/acsami.5b00183
ACS Appl. Mater. Interfaces 2015, 7, 12679−12687

a reducing atmosphere of N_2/H_2 gas for 20 min to optimize conductivity.[20]

Measurement. The sheet resistance of printed blanket films was measured using a 4-point probe system (Agilent 34401A). Printed lines were characterized by a precision semiconductor parameter analyzer (HP 4155A) using two point and four point configurations. Line morphology was measured with a 3D Laser Measuring Microscope (Olympus OLS4000) and a stylus profilometer (Veeco Dektak 6M) after the annealing step was completed. Line width and edge morphology were automatically extracted using a commercial software package (SuMMIT) for off-line analysis of optical microscope images. Optical transmittance was measured with a UV−visible spectrometer for normal incidence at wavelengths between 240 and 1040 nm with a spot size of diameter approximately 1 mm. XRD spectra were measured using an X-Pert Analytical system with 0.43° incidence angle. Uniaxial bending stress tests and fatigue tests were performed on printed lines and films using an automated setup consisting of a 3-axis linear stage. The thin glass substrate was clamped on one end with two flat aluminum plates while the free end was deflected. The radius of curvature was extracted using ImageJ.

■ ASSOCIATED CONTENT

Ⓢ Supporting Information

Table S1, comparison of the Scherrer equation estimated crystallite sizes for the ATO and ITO printed films; Table S2, comparison of the performance shown in this work versus other demonstrations of scalable additively patterned TCOs; Figure S1, full sweeps of shear stress versus shear rate for the printable inks used in this study, as well as creep tests of the time-relaxation behavior of ITO and ATO viscosity; Figure S2, a plot of surface tension of ITO sol−gels versus precursor concentration; Figure S3, zoomed images of the primary XRD peaks for ITO and ATO films of different concentrations; Figure S4, optical micrographs of the mesoscale uniformity of printed ITO and ATO films; Figure S5, SEM images of printed lines and films. The Supporting Information is available free of charge on the ACS Publications website at DOI: 10.1021/acsami.5b00183.

■ AUTHOR INFORMATION

Corresponding Author

*E-mail: viveks@eecs.berkeley.edu.

Author Contributions

The manuscript was written through contributions of all authors. All authors have given approval to the final version of the manuscript.

Notes

The authors declare no competing financial interest.

■ ACKNOWLEDGMENTS

Parts of this work were funded by BASF and the National Science Foundation. Will Scheideler is funded through an NSF fellowship. Rungrot Kitsomboonloha is funded through a Lam Research Fellowship.

■ ABBREVIATIONS

Ca = capillary number
TCO = transparent conducting oxide
ITO = tin-doped indium oxide
ATO = antimony-doped tin oxide
FOM = figure of merit (refers to Haacke figure of merit)

■ REFERENCES

(1) Krebs, F. C.; Gevorgyan, S. A.; Alstrup, J. A Roll-to-Roll Process to Flexible Polymer Solar Cells: Model Studies, Manufacture and Operational Stability Studies. *J. Mater. Chem.* **2009**, *19*, 5442−5451.
(2) Fortunato, E.; Ginley, D.; Hisono, H.; Paine, D. C. Transparent Conducting Oxides for Photovoltaics. *MRS Bull.* **2007**, *32*, 242−247.
(3) Andersson, A.; Johansson, N.; Broms, P.; Yu, N.; Lupo, D.; Salaneck, W. R. Fluorine Tin Oxide As an Alternative to Indium Tin Oxide in Polymer LEDs. *Adv. Mater.* **1998**, *10*, 859−863.
(4) Sierros, K. A.; Kukureka, S. N. Mechanical Integrity of Touch-Screen Components. *J. Soc. Inf. Dispersion* **2012**, *11*, 947−952.
(5) Eritt, M.; May, C.; Leo, K.; Toerker, M.; Radehaus, C. OLED Manufacturing for Large Area Lighting Applications. *Thin Solid Films* **2010**, *11*, 3042−3045.
(6) Katayama, M. TFT-LCD Technology. *Thin Solid Films* **1999**, *2*, 140−147.
(7) Betz, U.; Olsson, M. K.; Marthy, J.; Escola, M. F.; Atamny, F. Thin Films Engineering of Indium Tin Oxide: Large Area Flat Panel Displays Application. *Surf. Coat. Technol.* **2006**, *200*, 5751−5759.
(8) Ju, S.; Facchetti, A.; Xuan, Y.; Liu, J.; Ishikawa, F.; Ye, P.; Zhou, C.; Marks, T. J.; Janes, D. B. Fabrication of Fully Transparent Nanowire Transistors for Transparent and Flexible Electronics. *Nat. Nanotechnol.* **2007**, *2*, 378−384.
(9) Habas, S. E.; Platt, H. A. S.; van Hest, M. F. A. M.; Ginley, D. S. Low-Cost Inorganic Solar Cells: From Ink To Printed Device. *Chem. Rev.* **2010**, *110*, 6571−6594.
(10) U.S. Department of the Interior, U.S. Geological Survey. *Mineral Commodity Summaries 2014*; U.S. Geological Survey: Reston, VA, 2014.
(11) Arias, A. C.; MacKenzie, J. D.; McCulloch, I.; Rivnay, J.; Salleo, A. Materials and Applications for Large Area Electronics: Solution-Based Approaches. *Chem. Rev.* **2010**, *110*, 3−24.
(12) Lee, D. H.; Chang, Y.-J.; Herman, G. S.; Chang, C. H. A General Route to Printable High-Mobility Transparent Amorphous Oxides Semiconductors. *Adv. Mater.* **2007**, *19*, 843−847.
(13) Puetz, J.; Aegerter, M. A. Direct Gravure Printing of Indium Tin Oxide Nanoparticle Patterns on Polymer Foils. *Thin Solid Films* **2008**, *516*, 4495−4501.
(14) Puetz, J.; Heusing, S.; De Haro Moro, M.; Ahlstedt, C. M.; Aegerter, M. A. Gravure Printing of Transparent Conducting ITO Coatings for Display Applications. *Proc. SPIE* **2005**, *5963*, 405−412.
(15) Jorgensen, M.; Norrman, K.; Krebs, F. C. Stability/Degradation of Polymer Solar Cells. *Sol. Energy Mater. Sol. Cells* **2008**, *92*, 686−714.
(16) Zhou, Y.; Fuentes-Hermandez, C.; Shim, J.; Meyer, J.; Giordano, A. J.; Li, H.; Winget, P.; Papadopoulos, T.; Cheun, H.; Kim, J.; Fenoll, M.; Dindar, A.; Haske, W.; Najafabadi, E.; Khan, T. M.; Sojoudi, H.; Barlow, S.; Graham, S.; Bredas, J.-L.; Marder, S. R.; Kahn, A.; Kippelen, B. A Universal Method to Produce Low-Work Function Electrodes for Organic Electronics. *Science* **2012**, *336*, 327−332.
(17) Kitsomboonloha, R.; Morris, S. J. S.; Rong, X.; Subramanian, V. Femtoliter-scale patterning by High-Speed, Highly Scaled Inverse Gravure Printing. *Langmuir* **2012**, *28*, 16711−16723.
(18) Garner, S. M.; Wu, K. W.; Liao, Y. C.; Shiu, J. W.; Tsai, Y. S.; Chen, K. T.; Lai, Y. C.; Lai, C. C.; Lee, Y. Z.; Lin, J. C.; Li, X.; Cimo, P. Cholesteric Liquid Crystal Display With Flexible Glass Substrates. *J. Dispersion Technol.* **2013**, *9*, 644−650.
(19) Garner, S. M.; Glaesemann, S.; Li, X. Ultra-slim Flexible Glass for Roll-to-Roll Electronic Device Fabrication. *Appl. Phys. A: Mater. Sci. Process.* **2014**, *116*, 403−407.
(20) Chang, Z.; Li, w.; Li, R.; Zhang, Y.; Xu, G.; Cheng, H. Fabrication of Highly Transparent and Conductive Indium-Tin Oxide Thin Films with a High Figure of Merit via Solution Processing. *Langmuir* **2013**, *45*, 13836−13842.
(21) Ellmer, K. Past Achievements and Future Challenges in the Development of Optically Transparent Electrodes. *Nat. Photonics* **2012**, *6*, 809−817.
(22) Senguttuvan, T. D.; Malhotra, L. K. Sol−Gel Deposition of Pure and Antimony Doped Tin Dioxide Thin Films by Non-Alkoxide Precursors. *Thin Solid Films* **1996**, *1*, 22−28.

DOI: 10.1021/acsami.5b00183
ACS Appl. Mater. Interfaces 2015, 7, 12679−12687

(23) Avis, C.; Hwang, H. R.; Jang, J. Effect of Channel Layer Thickness on the Performance of Indium−Zinc−Tin Oxide Thin Film Transistors Manufactured by Inkjet Printing. *ACS Appl. Mater. Interfaces* **2014**, *6*, 10941−10945.
(24) Kim, D.; Jeong, Y.; Song, K.; Park, S. K.; Cao, G.; Moon, J. Inkjet-Printed Zinc Tin Oxide Thin-Film Transistor. *Langmuir* **2009**, *25*, 11149−11154.
(25) Kang, H.; Kitsomboonloha, R.; Jang, J.; Subramanian, V. High-Performance Printed Transistors Realized Using Femtoliter Gravure-Printed Sub-10-μm Metallic Nanoparticle Patterns and Highly Uniform Polymer Dielectric and Semiconductor Layer. *Adv. Mater.* **2012**, *24*, 3065−3069.
(26) Brinker, C. J.; Scherer, G. W. Sol → Gel → Glass: I. Gelation and Gel Structure. *J. Non-Cryst. Solids* **1985**, *70*, 301−322.
(27) Brinker, C. J. *Sol−Gel Science: The Physics and Chemistry of Sol−Gel Processing*; Scherer, G. W., Eds.; Academic Press: San Diego, CA, 1990; pp 204−207.
(28) Majumder, M.; Rendall, C. S.; Eukel, J. A.; Wang, J. Y. L.; Behabtu, N.; Pint, C. L.; Liu, T.-Y.; Orbaek, A. W.; Mirri, F.; Nam, J.; Barron, A. R.; Hauge, R. H.; Schmidt, H. K.; Pasquali, M. Overcoming the "Coffee-Stain" Effect by Compositional Marangoni-Flow-Assisted Drop-Drying. *J. Phys. Chem. B* **2012**, *116*, 6536−6542.
(29) Azizian, S.; Hemmati, M. Surface Tension of Binary mixtures of Ethanol + Ethylene Glycol from 20 to 50 °C. *J. Chem. Eng. Data* **2003**, *48*, 662−663.
(30) Zhang, G.; Liu, M. Preparation of Nanostructured Tin Oxide Using a Sol−Gel Process Based on Tin Tetrachloride and Ethylene Glycol. *J. Mater. Sci.* **1999**, *34*, 3213−3219.
(31) Ramanan, S. R. Dip-Coated ITO Thin-Films through Sol−Gel Process Using Metal Salts. *Thin Solid Films* **2001**, *389*, 207−212.
(32) Koebel, M. M.; Nadargi, D. Y.; Jimenez-Cadena, G.; Romanyuk, Y. E. Transparent, Conducting ATO Thin Films by Epoxide-Initiated Sol−Gel Chemistry: A Hightly Vesatile Route to Mixed-Metal Oxide Films. *ACS J. Appl. Mater. Interfaces* **2012**, *4*, 2464−2473.
(33) Popovic, J.; Tkalcec, E.; Grzeta, B.; Goebbert, C.; Ksenofontov, V.; Takeda, M. Z. Defect Structure Examination of Sn-Doped Indium Oxide (ITO). *Z. Kristallogr.* **2007**, *4*, 489−494.
(34) Grzeta, B.; Tkalcec, E.; Goebbert, C.; Takeda, M.; Takahashi, M.; Nomura, K.; Jaksic, M. Structural Studies of Nanocrystalline SnO_2 Doped with Antimony: XRD and Moessbauer Spectroscopy. *J. Phys. Chem. Solids* **2002**, *63*, 765−772.
(35) Auch, M. D. J; Soo, O. K.; Ewald, G.; Soo-Jin, C. Ultrathin Glass for Flexible OLED Application. *Thin Solid Films* **2002**, *417*, 57−50.
(36) Alzoubi, K.; Hamasha, M. M.; Lu, S.; Sammakia, B. Bending Fatigue Study of Sputtered ITO on Flexible Substrate. *J. Dispersion Sci. Technol.*. **2011**, *7*, 593−600.
(37) Jang, J. All Inkjet-Printed SnO_2/ZrO_2 Transistors. Ph.D. Thesis, University of California, Berkeley, CA, 2014.

DOI: 10.1021/acsami.5b00183
ACS Appl. Mater. Interfaces 2015, 7, 12679−12687